A new optimization procedure for the accurate characterization of thermal phase transformation curves based on controlled quenching experiments

Maurice Peterli[1,a], Minh-Trung Truong[1], Niko Manopulo[1] and Pavel Hora[1]

[1] *Institute of Virtual Manufacturing (IVP), ETH Zurich, Tannenstrasse 3, 8092, Zurich, Switzerland*

Abstract. Precise hardness and phase content prediction for quenched steel with the finite element method requires optimal material data, which is usually obtained from measured continuous cooling transformation (CCT) diagrams. However, most software packages that are able to predict final phase composition require time temperature transformation (TTT) diagrams. TTT diagrams can be calculated from the chemical composition of the material. With this methods the numerical prediction often result in deviations to reality. A newly developed optimization method can improve the accuracy of phase content and hardness prediction after quenching by optimizing the TTT diagram with measured data of controlled quenching experiments.

1 Introduction

Plenty of industrial components are subject to heat treatment in order to improve the parts mechanical properties. Prediction of the final phase content and hardness with finite element method can be difficult to achieve. Many software packages require a time temperature transformation diagram (TTT) which is difficult to obtain with standard measurement techniques. However it is more convenient to measure the continuous transformation diagram (CCT), which can be used to adjust the corresponding TTT diagram. Some deviations in the finite element results may come from this transformation, others can result from hard-won and imprecise phase content determination.

Realistic transformation kinetics are key to an accurate prediction of the current and final microstructure during quenching and can be represented with the TTT diagram. Although TTT diagrams contain only isothermal transformation data, they can be used to approximate the anisothermal quenching process by breaking it down into smaller isothermal steps. Together with the additivity principle, the theory "that of fictitious time" [1] and Sheil's [2] method, it is possible to access anisothermal transformation kinetics from isothermal data. Incubation and phase growth, which will only start when incubation is completed, are separated. The nucleation follows Sheil's summation and phase growth of diffusional transformations can be described with the Avrami equation [3, 4, 5], where y_n is the transformed volume fraction of bainite, ferrite or perlite, t is time , b and n are temperature dependent variables:

$$y_n = 1 - \exp(1 - bt^n) \qquad (1)$$

Diffusionless non-time dependent transformation from austenite to martensite can be expressed with the Koistinen and Marburger formula [6]:

$$y_{martensite} = y_{austenite}\{1 - \exp[-A(M_S - T)]\} \qquad (2)$$

$y_{austenite}$ represents the remaining austenite, T is the current temperature, A is a material dependent variable and M_S is the martensite start temperature. As soon as the temperature passes the M_S.temperature, the remaining austenite starts being transformed to martensite. There exist several tools to compute a TTT-diagram from the material's chemical composition and initial grain size [7, 8, 9]. The one used by the authors is presented in the following. The transformation kinetics can be predicted with the Kirkaldy method [10, 11], after the characteristic temperatures of phase change are estimated. The austenitization-end temperature ($A_{C3)}$ is averaged over the estimation method from Andrews [12] and Kasatkin [13]. Both are based on the chemical composition. The austenitization start temperature ($A_{C1)}$ is calculated with the Andrews model [12]. For the bainite-start-temperature B_S, the Kirkaldy model is used [10]. The martensite-start-temperature is averaged over Haynes [14] and Andrews [12].

The final hardness after quenching is calculated either by taking the final phase composition and match it with data from CCT-diagrams or by taking the transformation history into account. The latter can be done by determine the overall hardness through accumulation of the hardness values of each transformed phase component during each time step in the finite element simulation. The final hardness H can be formulated as [15]:

[a] Corresponding author: maurice.peterli@ivp.mavt.ethz.ch

$$H = \sum_k (\sum_i \Delta y_{ik} H_{ik}) \quad (3)$$

where y_{ik} is the phase component of phase i, that is formed during the time step k. H_{ik} is the hardness linked to phase i at the current temperature k.

This contribution aims to optimize the input data for finite element simulation of heat treatment processes for a better prediction of hardness and phase content in quenched parts.

2 Material Characterization

The material used in this work is a through-hardenable C60 steel. To characterize the thermo-mechanical properties, it is necessary to measure the standardized [16] CCT diagram. The experiments performed to obtain this data can later be used for the validation of the corresponding finite element simulation as later shown.

2.1 Measured CCT diagram

To characterize thermal characteristics a CCT-diagram was obtained with a DIL 805A/D quenching dilatometer from TA instruments (see Figure 1). Quenching experiments with the following cooling times (time from A_{C3}-temperature to 200°C) have been carried out; 10s, 15s, 20s, 40s, 60s, 100s, 200s, 500s and 1000s. By connecting the transformation points in the temperature-dilatation diagram, we get the phase regions and the martensite start temperature. With an additional slow heating experiment, the austenitization start and end temperatures are measured.

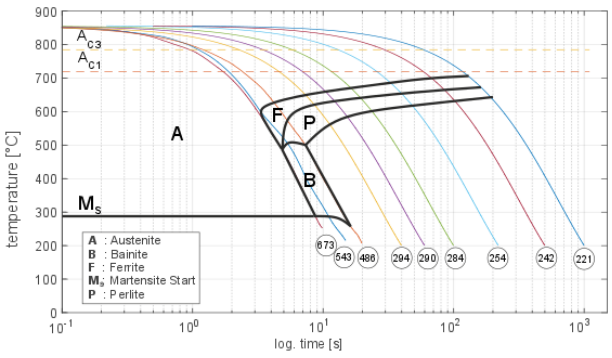

Figure 1. Measured-CCT diagram

The cylindrical specimen that were used for the quenching experiments were 4mm high and 4.5mm in diameter. After the experiments, final phase content and hardness (circled numbers at the end of each cooling curve) were measured.

2.2 Computed TTT-diagram

Additionally, the initial chemical composition of the material, the characteristic temperatures and grain size was determined as shown in Table 1.

Table 1. Chemical composition and characteristic temperatures

Fe	**C**	**Cr**	**Mn**	**Si**
98.209%	0.613%	0.27%	0.678%	0.204%
P	**Ni**	**Mo**	**S**	
0.017%	0.007%	0.001%	0.001%	
AC3	**AC1**	**BS**	**MS**	**Grain size**
785°C	720°C	572°C	261°C	7.5 µm

The following TTT diagram was calculated with the TTT-Generator from FORGE® using the material's chemical composition and grain size based on the method explained in the introduction. The computed TTT diagram is shown in Figure 2.

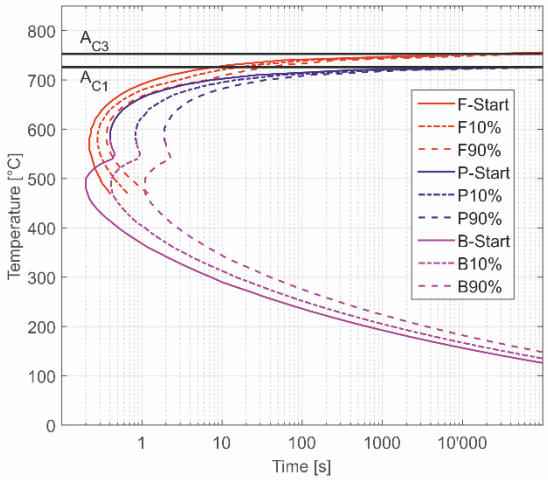

Figure 2. Computed TTT-diagram with the TTT Diagram Generator from FORGE®

This diagram is basis for the transformation kinetics during quenching. The solid lines represent the starting line for isothermal transformation for ferrite, perlite and bainite. The narrowly dotted line indicates the 10% and the coarse dotted line the 90% completion of transformation from austenite to the respective phase. For instance 10% bainite would have transformed from austenite after 15s, at 300°C under isothermal condition.

As mentioned in the introduction, hardness can be coupled with the phase transformation. The automatically generated temperature dependent hardness values for each phase is shown in Figure 3. For example the fraction of ferrite that is transformed from austenite to ferrite at 600°C has a hardness of 200HV. Every hardness of all fractions are summed-up for every time step according to equation (3) and result in the final hardness after quenching.

3 Quenching simulation

The finite element simulation was designed, so that the cylindrical specimens follow the measured temperature paths from the CTT diagram with FORGE® NxT 1.0.

After the simulations, final hardness and phase content was determined for all quenching times. The results of the experiments and the simulations are shown in Figure 4. Every dot represents a simulation or measurement for a certain quenching time.

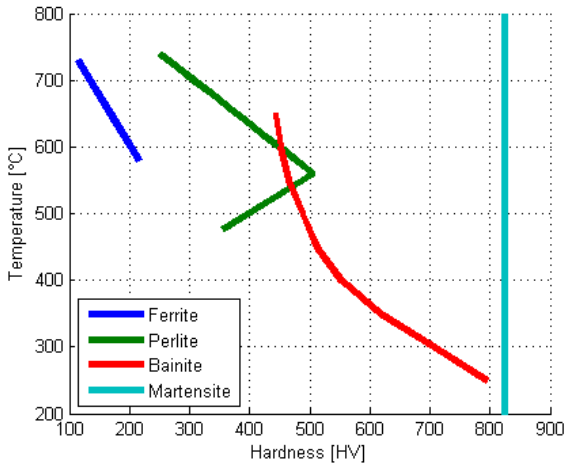

Figure 3. Calculated temperature dependent hardness

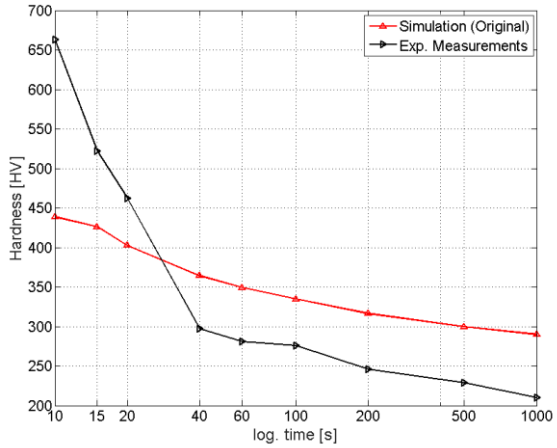

Figure 4. Measured versus simulated hardness

There is quite significant disagreement between measured and simulated hardness. The maximum hardness achieved in reality is over 200HV higher than in the simulation. This can be explained with the low martensite fraction of the simulation for fast cooling times. The micrographs show almost complete martensitic transformation for the quickest quenching specimen (10s). If we have look on the computed TTT-diagram in Figure 2 we can see that the ferrite, perlite and bainite 10% line is before the 1s mark, which means that it is impossible to get a full martensitic structure if the minimum quenching time is 10s. Those results show clearly that there is a potential for improvement.

4 Optimization process

For optimal prediction of phase content and hardness after quenching it is necessary to adjust the transformation curves in the TTT-diagram and change the hardness values, which are coupled with the phase evolution.

The determination of the phase composition by evaluating the corresponding micrographs is not trivial. Due to the light-dark contrast while using the etching method, the phase components and other metallic properties, such as grain boundaries, non-metallic inclusions or mixed phases etc., are visible. Furthermore, an accurate estimation of the percentage fractions of the phase composition is not possible with the naked eye. Although there exist picture analysis software to conquer this problem, the inaccuracies are still significant. A mathematical method can be used in order to identify the phase composition of the phase microstructure despite the uncertainties. A region-based optimization method can be used to identify the phase composition of the measured microstructure and optimizing the corresponding hardness values.

The uncertainties can be expressed with a minimum and a maximum possible phase fraction for each phase and quenching time.

4.1 Phase fraction and hardness optimization

The solution of the optimization problem is based on the assumption that a linear relationship between hardness values and the corresponding phase fractions exists. This is a simplification of reality and may cause some inaccuracies, but is necessary for the following optimization process. The linear dependency between phase fraction and hardness can be formulated as follows:

$$x_i h_F + x_{i+1} h_P + x_{i+2} h_B + x_{i+3} h_M = H_i \tag{4}$$

where h_F, h_P, h_B, h_M are the hardness values of the ferrite, pearlite, bainite and martensite phases. H_i is the macroscopic hardness for the corresponding quenching time i. $x_i, x_{i+1}, x_{i+2}, x_{i+3}$ represent the volume percentages of the phases, whereas their sum for each row results in 1:

$$x_i + x_{i+1} + x_{i+2} + x_{i+3} = 1 \tag{5}$$

Accordingly, a system of linear equations can be written as follows:

$$\begin{bmatrix} 0 & 0 & x_1 & x_2 \\ x_3 & 0 & x_4 & x_5 \\ x_6 & x_7 & x_8 & x_9 \\ x_{10} & x_{11} & 0 & 0 \\ x_{12} & x_{13} & 0 & 0 \\ x_{14} & x_{15} & 0 & 0 \\ x_{16} & x_{17} & 0 & 0 \\ x_{18} & x_{19} & 0 & 0 \\ x_{20} & x_{21} & 0 & 0 \end{bmatrix} * \begin{bmatrix} h_F \\ h_P \\ h_B \\ h_M \end{bmatrix} = \begin{bmatrix} 663 \\ 522 \\ 462 \\ 297 \\ 281 \\ 276 \\ 246 \\ 229 \\ 210 \end{bmatrix} \tag{6}$$

The left matrix contains the phase fractions. The first column is the ferrite, the second perlite, the third bainite and the last one the martensite fraction, that leads to the

measured hardness values (vector on the right) at the end of the quenching experiments taken from the CCT-diagram (Figure 1). A zero means that no trace of this phase was found in the micrograph. Hardness measurements are, in contrast to the phase volume percentages, easily and reproducible to measure. The hardness values h_F, h_P, h_B, h_M are unknown and will be optimized together with the phase fractions. Because of the assumption in equation (5), the fractions of all phases in a specimen have to equal 1, we can rewrite this system of equations to:

$$\begin{bmatrix} 0 & 0 & x_1 & 1-x_1 \\ x_2 & 0 & x_3 & 1-x_2+x_3 \\ x_4 & x_5 & x_6 & 1-(x_4+x_5+x_6) \\ x_7 & 1-x_7 & 0 & 0 \\ x_8 & 1-x_8 & 0 & 0 \\ x_9 & 1-x_9 & 0 & 0 \\ x_{10} & 1-x_{10} & 0 & 0 \\ x_{11} & 1-x_{11} & 0 & 0 \\ x_{12} & 1-x_{12} & 0 & 0 \end{bmatrix} * \begin{bmatrix} h_F \\ h_P \\ h_B \\ h_M \end{bmatrix} = \begin{bmatrix} 663 \\ 522 \\ 462 \\ 297 \\ 281 \\ 276 \\ 246 \\ 229 \\ 210 \end{bmatrix} \quad (7)$$

Note that although (7) is written as a matrix equation, the problem is nonlinear in the unknowns. Furthermore it is underdetermined as we have 9 equations for totally 16 unknowns (12 phase fractions and 4 hardness values). In order to further restrict the problem, micrographs have been visually inspected to determine upper and lower bounds for the phase volume fractions (Table 2). The problem has been subsequently solved using the constrained optimization functionality in Matlab (function fmincon). As expected only three of the phase fractions (x_5, x_{10} and x_{11}) have been actively optimized in addition to the four hardness values leading to a fully determined system. The rest of the values have been simply set to the boundary values satisfying the constraints equations.

Table 2 Phase fraction boundaries

Quenching time	Ferrite	Perlite	Bainite	Mart.
10s	0%	0%	5-10%	90-95%
15s	0-5%	0%	40-50%	45-60%
20s	0-15%	0-20%	50-60%	5-50%
40s	20-60%	40-80%	0%	0%
60s	20-60%	40-80%	0%	0%
100s	20-60%	40-80%	0%	0%
200s	20-60%	40-80%	0%	0%
500s	20-60%	40-80%	0%	0%
1000s	20-60%	40-80%	0%	0%

After running the optimization, we get the hardness for each phase, as well as the volume fraction $x_1 - x_{12}$ for the different specimens see Table 3 and Table 4:

Table 3 Optimized hardness for each phase

Phase	Hardness [HV]
Ferrite	137.35
Perlite	322.24
Bainite	517.76
Martensite	653.74

Table 4 Optimized phase fractions

x_1	x_2	x_3	x_4	x_5	x_6
0.05	0.05	0.5	0.15.	0.19	0.6
x_7	x_8	x_9	x_{10}	x_{11}	x_{12}
0.2	0.2	0.2	0.37	0.52	0.6

Now that phase fractions and hardness values are known, the TTT-diagram hast to be changed in order to simulate the quenching experiments accurately. Possible modifications and their influence on hardness and phase transformation are discussed in the following.

4.2 TTT-diagram modifications

As discussed in the introduction, the TTT diagrams used in the Forge simulations are calculated solely based on the chemical composition of the material. Although this is a good starting point in absence of further information, it is unable of accurately mimicking the behavior observed in the CCT experiments. In order to make sure that the TTT delivers results within the measured observation limit, a local modification strategy based on translation and stretching of the evaluated curves has been implemented.

Increasing the grain size leads to a general increase in the hardness values, because the ferrite phase fraction is reduced and therefore the perlite and bainite phase content are increased (see Figure 5). Conversely, the hardness values for all quenching times will be reduced when the grain size is decreased. This particular behavior applies only in the simulation and doesn't correspond to the observable grain size – hardness relationship [17, 18].

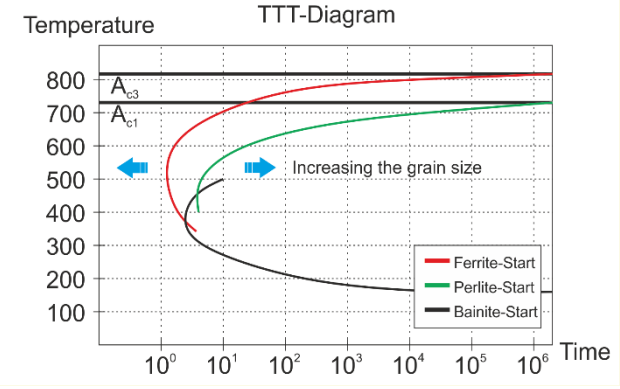

Figure 5. Influence of grain size

In order to influence the local hardness values, the TTT start curves must be modified (see Figure 6).

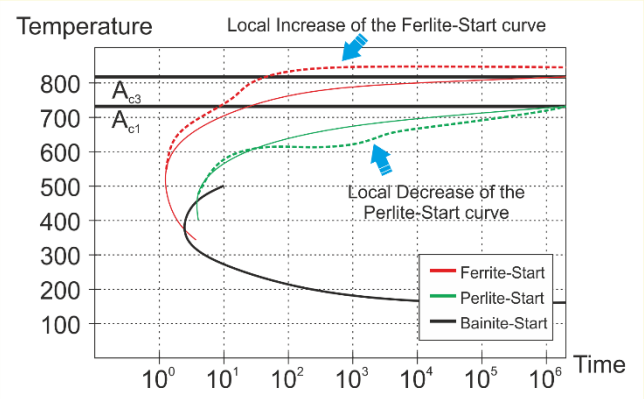

Figure 6. Modification of transformation curves

By lifting the ferrite-start curve, the hardness values for fast quenching (up to 20s) are reduced, lowering the curve leads to an increase of hardness. To change hardness for moderate cooling times (40s, 60s and 100s), the perlite start curve is most significant. The same rules as for the ferrite start curve applies. From micrographs it is known that bainite is only present for quenching times from 10s to 60s. Lifting the bainite curve results in a higher hardness after quenching and lowering the curve in a lesser hardness value.

The computed TTT-diagram (see Figure 2) was manually modified to fit the observations from the measured CCT-diagram (see Figure 1). Firstly the A_{C1}- and A_{C3}-temperature were corrected to fit the measurements. The transformation curves were generally shifted to the right, so that it is possible to transform martensite within 10s quenching time. The ferrite-start and bainite-start curve were lifted in order to have a lower hardness for moderate and higher hardness for faster quenching. The perlite transformation curves were not changed in shape. The final, optimized TTT-diagram is shown in Figure 7.

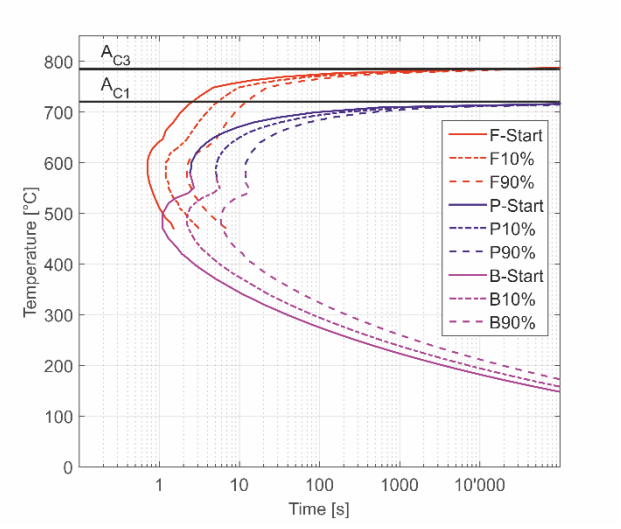

Figure 7. Optimized TTT-diagram

By combining the adjusted transformation kinetics and the simplified hardness values, an improved final hardness and phase prediction can be achieved as seen in Figure 8.

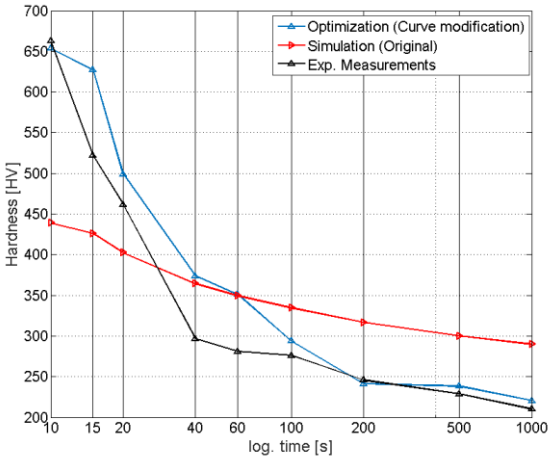

Figure 8. Optimized and original hardness prediction

There is a significant improvement for fast, mainly martensitic transformation (10s) and for slow ferrite/ perlite transformations (200-1000s). For quenching rates in between, further adjustments have to be done.

5 Conclusions

It was possible to show the flaws of using automatically generated TTT-diagrams based on the chemical composition for C60 steel. The impact of changes in the transformation curves on the final material hardness was also demonstrated. By optimizing the thermal material data with the presented optimization method, the prediction of final phase composition and hardness was more accurate for fast, pure martensitic and slow cooling rates.

With the proposed method it is no longer necessary to evaluate micrographs accurately, it is enough to define percentage boundaries for every phase. Additional effort has to be put in the optimization for more accurate results for all quenching rates.

References

1. W.I. Pumphrey, F.W. Jones, *ISIJ*, **189**, 137-144 (1948)
2. E. Scheil, *ZAAC*, **201(1),** 259–264 (1931)
3. M. Avrami, *J. Chem. Phys.* **7**, 1103-1112 (1939)
4. M. Avrami, *J. Chem. Phys.* **8(2)**, 212 (1940)
5. M. Avrami, Granulation, *J. Chem. Phys.* **9(2)**, 177 (1941)
6. D.P. Koistinen, R.E. Marburger, *Acta Mater.,* **7(1),** 59–60 (1959)
7. Z. Guo, J. Schillé, N. Saunders, et al, *2nd Int. Conf. on Heat Treat. and Surf. Eng. in Auto. Applic.* (2005)
8. N. Saunders, Z. Guo, AP Miodownik, J.P. Schillé, *J Mat Pro Software Literature* (2004)

9. P. Åkerström, M. Oldenburg, *J. Mater. Process. Technol*., **174(1-3)**, 399–406 (2006)
10. J.S. Kirkaldy, D. Venugopalan, *Phase Transformations in ferrous alloys*, 125-148 (1984)
11. B. Buchmayr, J.S. Kirkaldy, *J. Heat Treating*, **8**, 127–136 (1990)
12. K. W. Andrews, J. *Iron Steel Inst*, **203(7),** 721–727 (1965)
13. O.G. Kasatkin, B.B. Vinokur, V.L. Pilyushenko, *Met. Sci. Heat Treat.*, **26(1)**, 27–31 (1984)
14. W. Steven, A.G. Haynes, *J. Iron Steel Institute*, **183(8)**, 349–359 (1956)
15. *SEP 1680*, Aufstellung von Zeit-Temperatur-Umwandlungsschaubildern für Eisenlegierungen (1990)
16. M. Ehlers, Numerische und experimentelle Untersuchungen zur Eigenspannungs- und Verzugsausbildung beim martensitischen Härten von Stufenzylindern und Quadern in verdampfenden Flüssigkeiten, *Shaker* (2000)
17. N.J. Petch, *J. Iron Steel Inst.*, **174**, 25–28 (1953)
18. E.O. Hall, *Proc. Phys. Soc. Sect. B*, **64(9)**, 747 (1951)